Arm Inductance Quantification for Y-Matrix Modulated Modular Multilevel Converter

Yunting Liu
CURENT, Department of EECS
The University of Tennessee
Knoxville, TN, USA
yliu193@utk.edu

Fang Z. Peng
Center for Advanced Power Systems
Florida State University
Tallahassee, FL, USA

Leon M. Tolbert
CURENT, Department of EECS
The University of Tennessee
Knoxville, TN, USA

***Abstract*—Y-Matrix Modulated (YMM) Modular Multilevel Converter (MMC) was proposed recently. This modulation utilizes the self-voltage balancing capability of an MMC so that the conventional voltage balancing algorithm of MMC can be eliminated. YMM demonstrates that MMC has inherent self-voltage balancing capability. However, YMM assumes the voltage drop on the arm inductor to be zero to achieve MMC self-voltage balancing. This paper quantitatively justifies the zero voltage drop assumption for YMM based MMC and derives the general state-space model for MMC. Based on the general state-space model, the time-domain state variable dynamics are derived. The arm inductor assumption is justified by using the state variable dynamics. A criterion to determine the arm inductance value is given in this paper to quantify the zero voltage drop assumption. Simulation studies are provided to verify the state-space model derivation and the quantification of arm inductors.**

Keywords—Y-matrix modulation, modular multilevel converter, state-space model, arm inductor

I. INTRODUCTION

Y-Matrix Modulation (YMM) was proposed in [1] and [2]. This modulation utilizes the self-voltage balancing capability of MMC so that the conventional voltage balancing algorithm of MMC can be eliminated. To simplify the mathematical proof, the voltage drop on the arm inductor is assumed to be zero in [1]. This assumption indicates that the arm inductor should be very small. Therefore, the arm inductance needs to be quantified.

In order to quantify the arm inductance, a proper MMC model is needed to capture the dynamics of the arm inductor current. Many papers have modeled MMC for different purposes and scenarios. For example,

i) The MMC is modeled for external dynamics in order to understand the interaction between MMCs and other objectives (power grid, load, etc.) [3]–[5]. Normally, this type of model is for system level controller design.

ii) The MMC is modeled by arm or submodules in order to understand the internal state variables' dynamics [6]–[8]. Normally, this type of modeling serves internal state variable regulations.

iii) The MMC is modeled to evaluate a specific state variable at steady state [9]–[11]. This type of MMC modeling loses most of the dynamic properties of MMC but becomes an effective guidance for parameter design.

iv) The MMC is modeled for real-time simulation purpose [12]–[14]. The existing literature proposes numerous simplified and computationally-efficient equivalent models for MMC to meet with the fast calculation needed for real-time simulations.

Most of the models developed so far differ from each other on the basis of different assumptions and simplification. This makes them unsuitable for capturing the dynamics of arm inductor current. Wang et. [15] proposed a state-space switching model, which is derived from an accurate mathematical model without losing any characteristics of MMC. However, the aim of [15] is to develop a control to minimize the submodule capacitance and arm inductance. Therefore, the state variables selected in [15] are control oriented.

This paper derives a comprehensive state-space model for an MMC system. With this state-space model, the dynamics of the self-voltage balancing of MMC system could be well captured. The accuracy of the state-space model is validated by comparing with MATLAB/Simulink simulation. Based on the state-space model of MMC, the time-domain analytical formulation of state variables is derived. The analytical solutions are used to quantify the arm inductance needed for the zero voltage drop assumption. The quantification of arm inductance is verified with simulation results. This paper is organized as follows. Section II reviews the operating principle of YMM based MMC. Section III derives the general state-space model of MMC. Section IV justifies the arm inductor assumption that guarantees the self-balancing capability of MMC. Section V provides some simulation results to verify the state-space model and the quantification of arm inductance.

II. REVIEW OF Y MATRIX MODULATION

An N-level MMC is shown in Fig. 1. An N-level MMC contains $N-1$ submodules in the upper arm and $N-1$ submodules in the lower arm. For an N-level MMC, there are $N-1$, and only $N-1$, out of $2N-2$ submodules in insertion mode (current passes through capacitor) at all times. The other $N-1$ submodules are at bypass mode meanwhile. Therefore, there are

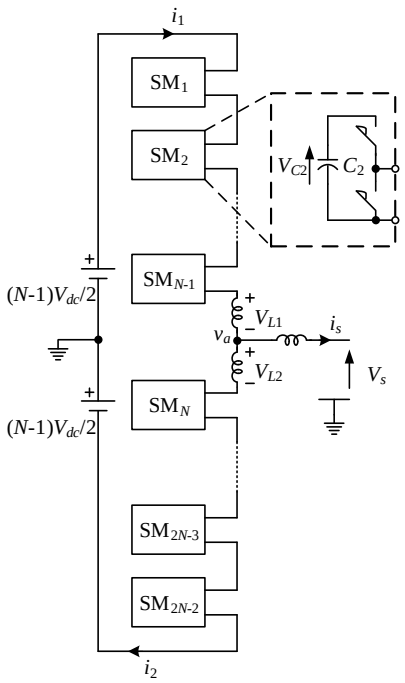

Fig. 1. *N*-level MMC circuit.

N possible levels for pole voltage v_a. The numbering of levels in an *N*-level MMC is shown in Fig. 2.

Define $\mathbf{Y}^{(N)}$ to be the *N*-level MMC submodule pattern space. Define a space $\mathbb{m}$ *s.t.* $\mathbb{m} \subseteq \mathbb{Z} \cap [1, N]$. $\mathbb{Z}$ is the set of all integers $\left(\mathbf{Y}_n^{(N)}\right)_{i\times j} \subset \mathbf{Y}$ is the *n*-th level submodule pattern space, where

$$i = \binom{n-1}{N-2} \cdot \binom{N-n-1}{N-2}, j = 2N-2 \; \forall n \in \mathbb{m}. \quad (1)$$

Ref [1] proves that

$$\exists\left(\hat{\mathbf{Y}}_n^{(N)}\right)_{k\times j} \subset \mathbf{Y}_n^{(N)} \quad (2)$$

s.t.

$$k = 2N-3 \;\cap\; rank\begin{bmatrix}\hat{\mathbf{Y}}_n^{(N)} \\ \hat{\mathbf{Y}}_{n+1}^{(N)}\end{bmatrix} = j \; \forall n \in \mathbb{m} \cap n \neq N. \quad (3)$$

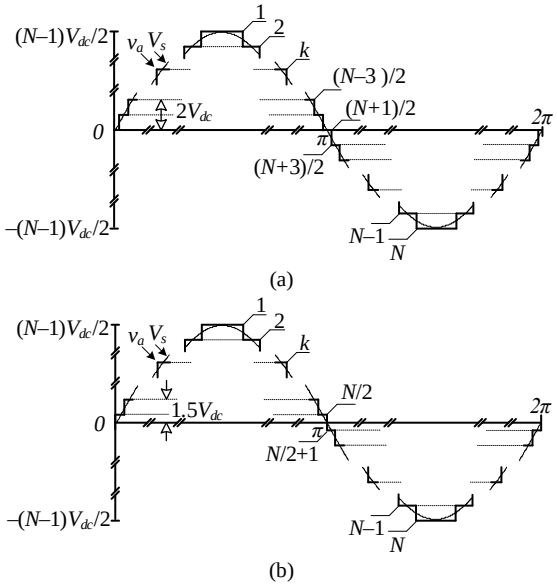

Fig. 2. Numbering of levels in an *N*-level MMC, when (a) *N* is an odd number; and (b) *N* is an even number [1].

MMC achieves self-balancing when it exhausts the submodule pattern space $\left[\left(\hat{\mathbf{Y}}_n^{(N)}\right)^{\mathrm{T}} \quad \left(\hat{\mathbf{Y}}_{n+1}^{(N)}\right)^{\mathrm{T}}\right]^{\mathrm{T}}$.

In order to exhaust the submodule pattern space, the Y-matrix pointer $f: \mathbb{m} \to \hat{\mathbf{Y}}_n^{(N)}$ rotates within a submodule pattern space $\hat{\mathbf{Y}}_n^{(N)}$ when level pointer $u: \mathbb{R} \to \mathbb{m}$ returns level *n*. *f* returns with the current switching pattern that *f* points to. Then, *f* is assigned to the next row vector in $\hat{\mathbf{Y}}_n^{(N)}$ and waits for *u* returning to *n*. The YMM for *N*-level MMC can also be explained with the aid of Fig. 3.

III. Derivation of State-Space Model for Y-Matrix Modulated MMC

Define the state variables to be

$$\mathbf{X} = \begin{bmatrix} x_1 \\ x_2 \\ x_3 \\ x_4 \\ \vdots \\ x_{2N} \end{bmatrix} = \begin{bmatrix} i_1 \\ i_2 \\ V_{C1} \\ V_{C2} \\ \vdots \\ V_{C(2N-2)} \end{bmatrix}. \quad (4)$$

$$\mathbf{A} = \begin{bmatrix} -\frac{R}{2L} & -\frac{R}{2L} & y_1\cdot\left(-\frac{1}{2L}\right) & y_2\cdot\left(-\frac{1}{2L}\right) & \cdots & y_{2N-2}\cdot\left(-\frac{1}{2L}\right) \\ -\frac{R}{2L} & -\frac{R}{2L} & y_1\cdot\left(-\frac{1}{2L}\right) & y_2\cdot\left(-\frac{1}{2L}\right) & \cdots & y_{2N-2}\cdot\left(-\frac{1}{2L}\right) \\ y_1\cdot\left(\frac{1}{C_1}\right) & 0 & 0 & 0 & 0 & 0 \\ \vdots & \vdots & \vdots & \vdots & \vdots & \vdots \\ y_{N-1}\cdot\left(\frac{1}{C_{N-1}}\right) & 0 & 0 & 0 & 0 & 0 \\ 0 & y_N\cdot\left(\frac{1}{C_N}\right) & 0 & 0 & 0 & 0 \\ \vdots & \vdots & \vdots & \vdots & \vdots & \vdots \\ 0 & y_{2N-2}\cdot\left(\frac{1}{C_{2N-2}}\right) & 0 & 0 & 0 & 0 \end{bmatrix}_{2N\times 2N} \quad (6)$$

where y_m is an element of the switching pattern $\hat{\mathbf{Y}}^{(N)}$.

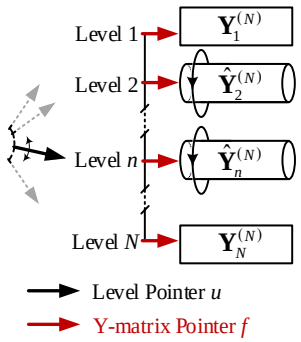

Fig. 3. Y-matrix modulation for *N*-level MMC [2].

The state equation is as follows,

$$\dot{\mathbf{X}} = \mathbf{A} \cdot \mathbf{X} + \mathbf{B} \cdot \mathbf{U}, \tag{5}$$

where **A** is shown in (6), and

$$\mathbf{B} = \begin{bmatrix} \frac{1}{2L} & \frac{1}{2} \\ \frac{1}{2L} & -\frac{1}{2} \\ 0 & 0 \\ 0 & 0 \\ \vdots & \vdots \\ 0 & 0 \end{bmatrix}_{2N\times 2}, \tag{7}$$

$$\mathbf{U} = \begin{bmatrix} V_{dc} \\ \frac{di_s}{dt} \end{bmatrix}. \tag{8}$$

The coefficient matrix could be decomposed as follows,

$$\mathbf{A} = \begin{bmatrix} \mathbf{A}_R & \mathbf{A}_L \\ \mathbf{A}_C & \mathbf{0} \end{bmatrix}. \tag{9}$$

where

$$\mathbf{A}_L = \begin{bmatrix} -\frac{1}{2L} \\ -\frac{1}{2L} \end{bmatrix} \cdot [y_1 \quad y_2 \quad \cdots \quad y_{2N-2}] = \widehat{\mathbf{A}}_L \cdot \mathbf{Y}_y^{(N)}. \tag{10}$$

$$\mathbf{A}_C = [\widehat{\mathbf{A}}_C \quad \overline{\mathbf{A}}_C]. \tag{11}$$

$$\widehat{\mathbf{A}}_C = diag\left(\begin{bmatrix} \frac{1}{C_1} \\ \vdots \\ \frac{1}{C_{N-1}} \\ 0 \\ \vdots \\ 0 \end{bmatrix}_{(2N-2)\times 1} \cdot [y_1 \quad y_2 \quad \cdots \quad y_{2N-2}] \right)$$
$$= diag\left(\widehat{\mathbf{A}}'_C \cdot \mathbf{Y}_y^{(N)}\right). \tag{12}$$

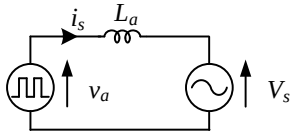

Fig. 4. Load inductor voltage modeling.

$$\overline{\mathbf{A}}_C = diag\left(\begin{bmatrix} 0 \\ \vdots \\ 0 \\ \frac{1}{C_N} \\ \vdots \\ \frac{1}{C_{2N-2}} \end{bmatrix}_{(2N-2)\times 1} \cdot [y_1 \quad y_2 \quad \cdots \quad y_{2N-2}] \right)$$
$$= diag\left(\overline{\mathbf{A}}'_C \cdot \mathbf{Y}_y^{(N)}\right). \tag{13}$$

diag returns with a column vector of the main diagonal elements of the objective matrix. $\widehat{\mathbf{A}}_L$ contains the parameters from arm inductance.

$\widehat{\mathbf{A}}'_C$ and $\overline{\mathbf{A}}'_C$ contain the parameters from submodule capacitance. $\widehat{\mathbf{A}}'_C$ contain the parameters from upper arm submodules. $\overline{\mathbf{A}}'_C$ contains the parameters from lower arm submodules. *R* is the arm equivalent resistance. *L* is the arm inductance.

Note that **U** contains di_s/dt, which is proportional to the voltage across the load inductor.

$$L_a \frac{di_s}{dt} = v_a - V_s, \tag{14}$$

which is modeled in Fig. 4.

Replacing the di_s/dt in (8) by (14) yields

$$\mathbf{U} = \begin{bmatrix} V_{dc} \\ \frac{1}{L_a}(v_a - V_s) \end{bmatrix}. \tag{15}$$

IV. Arm Inductor Assumption and Quantification

The transient component should be damped to zero if resistance *R* exists in the circuit. In a real MMC prototype, the switching loss and conduction loss is unavoidable. YMM-based MMC operates at high switching frequency for all submodules. Therefore, 2-4% power loss exists, and this power loss can be modeled by resistance.

In order to assume the inductor voltage to be zero, the transient needs to be damped within the switching period T_{sw}. From (6), the damping time constant of the transient, which is located at the top left corner of the matrix, is

$$\tau = 2\,L/R \tag{16}$$

where *R* is the equivalent converter loss. Therefore, $\tau < T_{sw}$ is the condition to ensure that the arm inductor assumption holds.

When *L* is small, e.g., zero, then the above condition will automatically hold, and at each switching instant, charging balance occurs. However, the charging and discharging current would be inrush (or impulse) current that may not be good for devices and cause a fault. Then in order to limit inrush charging/discharging current, we have to have a minimum inductance to make sure the inrush charging/discharging current is below 2 times rated load current.

V. Case Study

A. State-Space Model Verification

To verify the state-space model derivation, the differential equation (5) of the state-space model is discretized as follows,

$$d\mathbf{X} = \mathbf{A} \cdot \mathbf{X} \cdot dt + \mathbf{B} \cdot \mathbf{U} \cdot dt, \quad (17)$$

$$\mathbf{X}(k) = \mathbf{A}(k-1) \cdot \mathbf{X}(k-1) \cdot \Delta T + \mathbf{B} \cdot \mathbf{U}(k-1) \cdot \Delta T + \mathbf{X}(k-1), \quad (18)$$

The system matrix $\mathbf{A}$ is a function of submodule patterns. The submodule pattern space of this paper follows the one discussed in [2].

A simulation of a single-phase eleven-level MMC model in MATLAB/Simulink is conducted in comparison with the state-space model. The simulation circuit is shown in Fig. 5. The key parameters of the system are summarized in Table I. Ideal switches, inductors, and capacitors with no parasitic parameters as well as ideal voltage sources were used. Any controller delays are not included in the model. In the simulation setup, discrete-Tustin/Backward Euler (TBE) with a sample time of 0.167 µs is selected. The initial values of capacitor voltages are 1000 V. In Simulink, the MMC inductor currents are dependent states, and therefore, the initial values of the inductor current are determined by MATLAB/Simulink.

The comparison results are shown in Fig. 6. It shows the Simulink simulation along with the state-space model in four fundamental cycles. The proposed state-space model matches with the simulation. This indicates that the mathematical derivation of the proposed model is correct.

TABLE I. 11-Level MMC State-Space Model and Simulation.

Fundamental Frequency, f_0	60 Hz
Switching Frequency, f_{sw}	60 kHz
DC-Bus Voltage, V_{dc}	10 kV
Load Resistance, R_{load}	62 Ω
Line Inductance, L_{line}	1 mH
Arm Inductance, L_{arm}	0.1 µH
Stray Resistance, R_{stray}	0.2 Ω
Submodule Capacitance, C_i	770 µF
Number of Submodules per Arm	10

where i = 1, 2, …, 20.

TABLE II. 3-Level MMC Arm Inductor Justification Simulation.

Apparent Power, S	100 kVA
Fundamental Frequency, f_0	60 Hz
Switching Frequency, f_{sw}	5 kHz
DC-Bus Voltage, V_{dc}	2000 V
Phase Voltage, V_a, V_b, V_c	643 V
Line Current, I_a, I_b, I_c	52 A
Load Resistance, R_{load}	12.4 Ω
Line Inductance, L_{line}	4 mH
Sub-Module Capacitance, C_i	85 µF
Number of Sub-Modules per Arm	2

where i = 1, 2, …, 12.

TABLE III. MMC Arm Inductor Parameters.

	Arm Inductance, L	Equivalent Resistance, R
$\tau / T_{sw} = 0.25$	10 µH	0.4 Ω (3.2% p.u.)
$\tau / T_{sw} = 1$	40 µH	0.4 Ω (3.2% p.u.)
$\tau / T_{sw} = 10$	400 µH	0.4 Ω (3.2% p.u.)

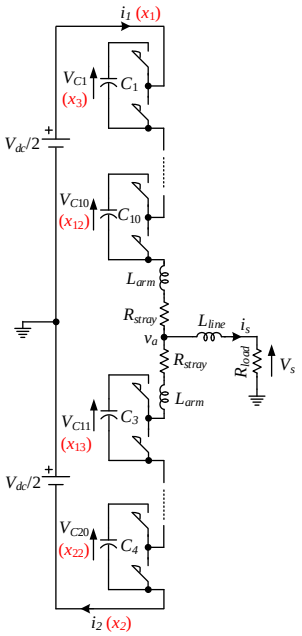

Fig. 5. Eleven-level single-phase MMC circuit for state-space model study.

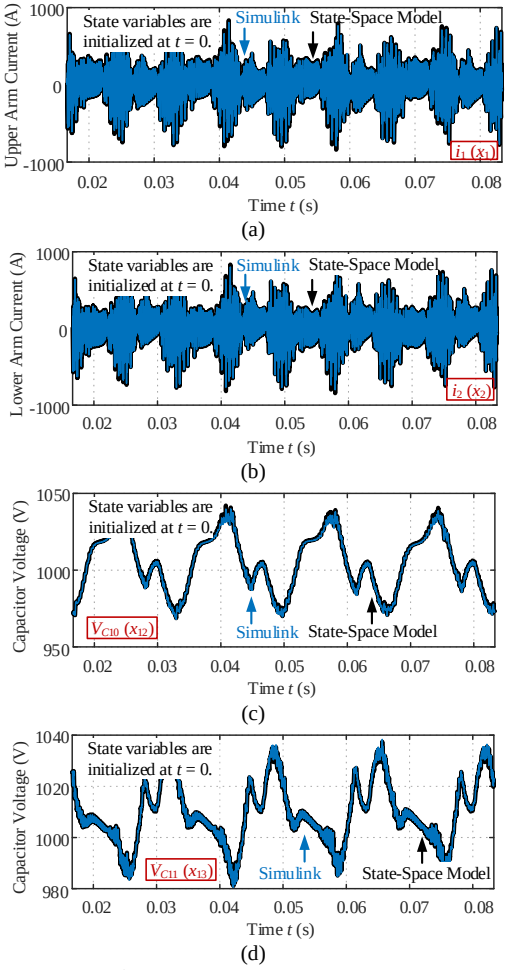

Fig. 6. Comparison of simulation and state-space model. (a) Upper arm current; (b) lower arm current; (c) capacitor voltage V_{C10}; (d) capacitor voltage V_{C11}.

B. *Arm Inductance Verification*

In this Section, several simulations with various arm inductances are examined to verify the analysis in Section IV. The simulation topology is shown in Fig. 7. The key parameters of the MMC are summarized in Table II. The time constants and the corresponding inductor value of the cases under study in this Section are summarized in Table III.

Three sets of arm inductors and time constants are tested in the simulation. Fig. 8 shows the output voltage of MMC with respect to different arm inductance. Fig. 9 shows the capacitor voltage of MMC with respect to different arm inductance. Fig. 10 shows the arm inductor current of MMC with respect to different arm inductance. Fig. 8(a), Fig. 9(a) and Fig. 10(a) show the first case, which is τ / T_{sw} = 0.25. The zero voltage drop assumption holds in these cases. The output voltage has less distortion. The capacitor voltage is well balanced. The capacitor voltage ripple is well constrained. The arm inductor current is limited within 2 times the load current. Fig. 8(b), Fig. 9(b) and Fig. 10(b) show the second case, which is τ / T_{sw} = 1. This case is at the boundary of analysis in Section IV. The output voltage has relatively larger distortion compared to the first case. The capacitor voltage is still balanced. The capacitor voltage ripple increases to $\pm$ 20% which is normally regarded as at the boundary of normal and abnormal operation. The arm inductor current is limited within 2 times the load current as well. Fig. 8(c), Fig. 9(c) and Fig. 10(c) show the third case simulation, which is τ / T_{sw} = 10. This case is out of the time constant range from Section IV. The output voltage has more distortion compared to Fig. 8(a) and (b). The capacitor voltage diverges from the 1000-V nominal value. The zero voltage drop assumption does not hold in this case. MMC falls into the abnormal operation. These three cases verify that the arm inductor assumption justification in Section IV.

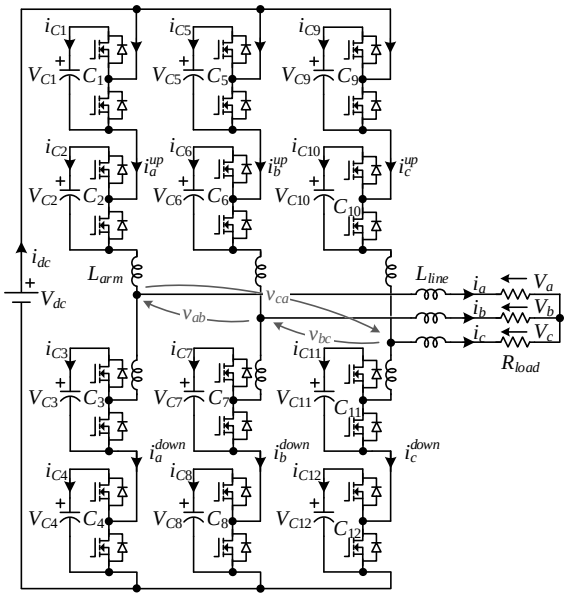

Fig. 7. Three-level MMC simulation topology.

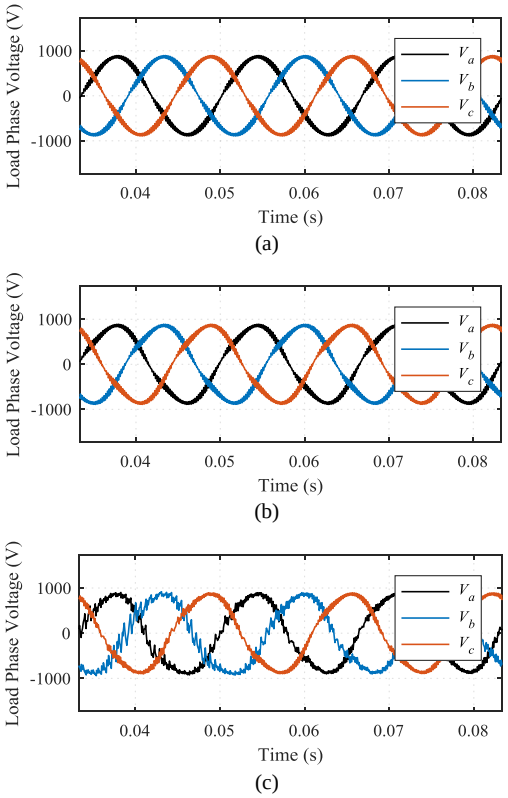

Fig. 8. Three-level MMC load voltage. (a) τ / T_{sw} = 0.25; (b) τ / T_{sw} = 1 and (c) τ / T_{sw} = 10.

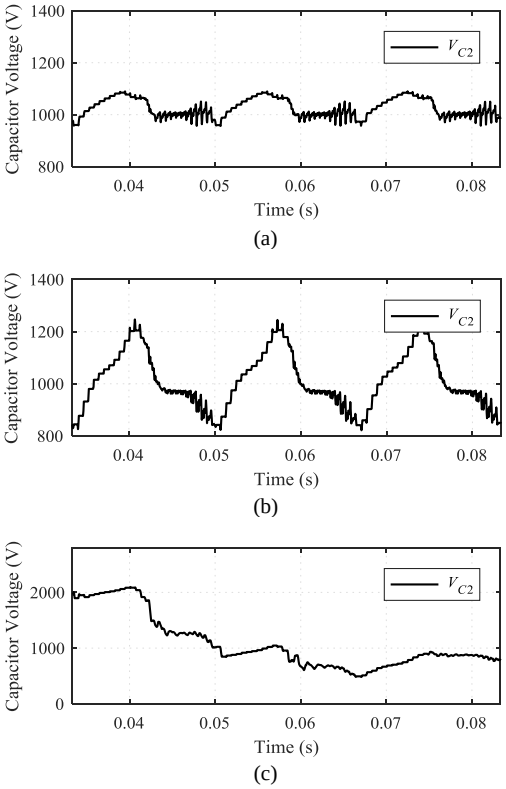

Fig. 9. Submodule capacitor voltage. (a) τ / T_{sw} = 0.25; (b) τ / T_{sw} = 1 and (c) τ / T_{sw} = 10.

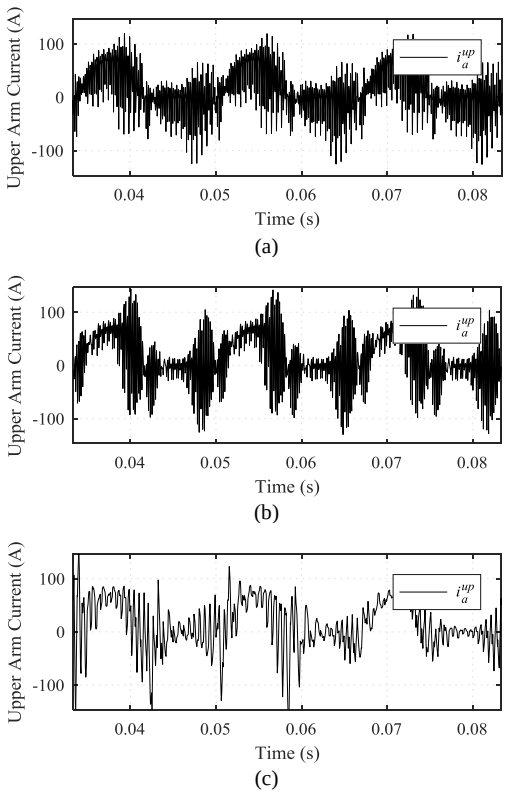

Fig. 10. Upper arm current. (a) $\tau / T_{sw} = 0.25$; (b) $\tau / T_{sw} = 1$ and (c) $\tau / T_{sw} = 10$.

VI. Conclusion

This paper quantitively justifies the arm inductance value to guarantee the voltage drop assumption for YMM based MMC. This paper first derives the general state space model for MMC dynamics. Then the arm inductor value constraint is derived based on the state space model. The derivation shows that the zero voltage drop assumption holds when the time constant $\tau = 2L/R < T_{sw}$. This criterion is validated by simulation study. The simulation results show that the waveform distortion increases when τ passes this constraint. A case with $\tau = 10$ shows that the capacitor voltages diverge in this condition.

Acknowledgement

This work was supported primarily by the Engineering Research Center Program of the National Science Foundation and Department of Energy under NSF Award Number EEC-1041877 and the CURENT Industry Partnership Program.

References

[1] Y. Liu and F. Z. Peng, "A modular multilevel converter with self-voltage balancing -part I: mathematical proof," *IEEE J. Emerg. Sel. Top. Power Electron.*, vol. 8, no. 2, pp. 1117-1125, June 2020.

[2] Y. Liu and F. Z. Peng, "A modular multilevel converter with self-voltage balancing -part II: y-matrix modulation," *IEEE J. Emerg. Sel. Top. Power Electron.*, vol. 8, no. 2, pp. 1126-1133, June 2020.

[3] J. Hu, J. Zhu, and M. Wan, "Modeling and analysis of modular multilevel converter in dc voltage control timescale," *IEEE Trans. Ind. Electron.*, vol. 66, no. 8, pp. 6449-6459, 2019.

[4] J. Lyu, X. Cai, and M. Molinas, "Optimal design of controller parameters for improving the stability of MMC-HVDC for wind farm integration," *IEEE J. Emerg. Sel. Top. Power Electron.*, vol. 6, no. 1, pp. 40–53, 2018.

[5] H. Yuan, X. Yuan, and J. Hu, "Modeling of grid-connected VSCs for power system small-signal stability analysis in dc-link voltage control timescale," *IEEE Trans. Power Syst.*, vol. 32, no. 5, pp. 3981–3991, 2017.

[6] A. Antonopoulos, L. Ängquist, L. Harnefors, K. Ilves, and H. Nee, "Global asymptotic stability of modular multilevel converters," *IEEE Trans. Ind. Electron.*, vol. 61, no. 2, pp. 603–612, 2014.

[7] L. Ängquist, A. Antonopoulos, D. Siemaszko, K. Ilves, M. Vasiladiotis, and H. Nee, "Open-loop control of modular multilevel converters using estimation of stored energy," *IEEE Trans. Ind. Appl.*, vol. 47, no. 6, pp. 2516–2524, 2011.

[8] Z. Xu, B. Li, S. Wang, S. Zhang, and D. Xu, "Generalized single-phase harmonic state space modeling of the modular multilevel converter with zero-sequence voltage compensation," *IEEE Trans. Ind. Electron.*, vol. 66, no. 8, pp. 6416-6426, 2019.

[9] Z. Liu, K.-J. Li, J. Wang, Z. Javid, M. Wang, and K. Sun, "Research on capacitance selection for modular multilevel converter," *IEEE Trans. Power Electron.*, vol. 34, no. 9, pp. 8417-8434, 2019.

[10] L. M. Cunico, G. Lambert, R. P. Dacol, S. V. G. Oliveira, and Y. R. De Novaes, "Parameters design for modular multilevel converter (MMC)," *Brazilian Power Electron. Conf. COBEP Proc.*, pp. 264–270, 2013.

[11] S. P. Engel and R. W. De Doncker, "Control of the modular multi-level converter for minimized cell capacitance," *Proc. 14th Eur. Conf. Power Electron. Appl.*, pp. 1–10, Birmingham, UK, 2011.

[12] H. Saad, J. Peralta, S. Dennetière, J. Mahseredjian, J. Jatskevich, J. A. Martinez, A. Davoudi, M. Saeedifard, V. Sood, X. Wang, J. Cano, A. Mehrizi-Sani, "Dynamic averaged and simplified models for MMC-based HVDC transmission systems," *IEEE Trans. Power Deliv.*, vol. 28, no. 3, pp. 1723–1730, 2013.

[13] U. N. Gnanarathna, A. M. Gole, and R. P. Jayasinghe, "Efficient modeling of modular multilevel HVDC converters (MMC) on electromagnetic transient simulation programs," *IEEE Trans. Power Del.*, vol. 26, no. 1, pp. 316–324, 2011.

[14] H. Saad, S. Dennetière, J. Mahseredjian, P. Delarue, X. Guillaud, J. Peralta, S. Nguefeu, "Modular multilevel converter models for electromagnetic transients," *IEEE Trans. Power Deliv.*, vol. 29, no. 3, pp. 1481–1489, 2014.

[15] J. Wang, R. Burgos, and D. Boroyevich, "Switching-cycle state-space modeling and control of the modular multilevel converter," *IEEE J. Emerg. Sel. Top. Power Electron.*, vol. 2, no. 4, pp. 1159–1170, 2014.